ISSN 0036-0244, Russian Journal of Physical Chemistry A, 2020, Vol. 94, No. 11, pp. 1510–1516. © Pleiades Publishing, Ltd., 2020.
Russian Text © The Author(s), 2020, published in Zhurnal Fizicheskoi Khimii, 2020, Vol. 94, No. 11, pp. 1608–1615.

CHEMICAL KINETICS AND CATALYSIS

Iron Dispersed on a Carbon Substrate Based on Shadbush (*Amenanchier*) Wood Pulp: Carbidizing Bismuth-Promoted Fe-Containing Catalysts for the Hydrogenation of CO

G. V. Pankina[a,*], P. A. Chernavskii[a], A. N. Kharlanov[a], A. V. Malkov[b], and V. V. Lunin[a]

[a] *Faculty of Chemistry, Moscow State University, Moscow, 119991 Russia*

[b] *Laverov Federal Center for Integrated Arctic Research, Russian Academy of Sciences, Arkhangelsk, 163000 Russia*

**e-mail: pankina5151@inbox.ru*

Received February 12, 2020; revised February 12, 2020; accepted March 17, 2020

Abstract—Carbon material (CM) based on shadbush C_{Am} (*Amenanchier*) wood pulp and a mixture of C_{Am} + AMS, where AMS is aluminum magnesium spinel, are used as a substrate for a Fe-containing catalyst promoted by Bi (0.6 wt %) for the hydrogenation of CO. The dynamics of the formation of iron carbides during the activation of iron oxides supported on the CM and CM–aluminum magnesium spinel mixture is studied, along with the effect bismuth has on this process. It is found that they already have nonzero magnetization at the stage of preparing the catalysts. It is shown that with Fe/C_{Am}, only Hägg carbide forms in a medium of CO/H_2 (1 : 1), while a mixture of Hägg carbides and ε'-$Fe_{2.2}C$ forms when using $Fe/(C_{Am}$ + AMS). The promotion of the $Fe/(C_{Am}$ + AMS) catalyst by bismuth substantially increases the amount of formed Hägg carbide and affects the amount of ε'-$Fe_{2.2}C$ negligibly.

Keywords: carbon material, aluminum magnesium spinel, promotion, carbides, in situ magnetometric method

DOI: 10.1134/S0036024420110266

INTRODUCTION

Over the last decade, great many works have been devoted to the synthesis and use of carbon materials (CMs) obtained from such renewable sources of vegetable origin as the pulp of various wood species, rice husks, wastes from coffee manufacturers, and biomass [1–3].

It is known that the production of CMs from natural renewable sources excludes the use of quite expensive chemicals and solves the environmentally relevant problem of disposing of wood pulp. The cost of producing CMs from natural feedstock is relatively low. Carbon materials are in demand as the substrates for Fe- and Co-containing catalysts in the selective production of C_2–C_4 alkenes, C_5 hydrocarbons, and liquid paraffins during the hydrogenation of CO or Fischer–Tropsch synthesis (FTS), in which synthesis gas H_2/CO is obtained from biomass, coal, and natural and shale gases.

When choosing the substrate for metal-containing catalysts, it is important to remember there should be no oxide–oxide interaction between a porous substrate and an active component that could lead to the formation of hard-to-reduce intermediate compounds, e.g., spinel structures that are virtually irreducible at the relevant temperatures in the stage of preparing the catalysts [4]. Such substrates clearly include aluminum magnesium spinels of different stoichiometric compositions. CMs do not generally interact with active components.

Iron oxides supported on a carbon matrix or aluminum magnesium spinel are normally composites with large specific surfaces and developed porous structures that effectively adsorb gases and chemical compounds dissolved in fluids [5]. Such nanomaterials are characterized by a high fraction of surface atoms and metastable morphology with a local minimum of free energy.

It is currently thought that metal (iron, cobalt) carbides of different stoichiometric compositions act as active sites during the hydrogenation of CO [6–8]. In the case of iron-containing catalysts, these are cementite Fe_2C and Hägg carbide χ-Fe_5C_2 [6–9]. Niemantsverdriet et al. confirmed the hypothesis that Hägg carbide χ-Fe_5C_2 actively participates in the FTS reaction [10]. Experimental data obtained by Khodakov et al. showed that when using a carbon substrate in an iron-containing catalyst, high activity is achieved through the considerable reactivity and fast regenerating capacity of Hägg carbide [9]. The carbon of the substrate actively participates in the growth of the carbon chain. It has been found that fairly stable magne-

tite forms upon activating an Fe/CNT catalyst in a CO flow at 350°C. Due to the close contact between magnetite and the carbon of the substrate, a positive effect is observed in the catalytic hydrogenation reaction of CO [9].

In studying the dynamics of carbidizing, it has been noted that only Hägg carbide forms upon the activation of $Fe/MgAl_2O_4$ catalysts in the synthesis gas [11]. It is noteworthy that when choosing aluminum magnesium spinels that differ from one another in the values of their specific surfaces by almost an order of magnitude (23 and 185 m^2/g), the amount of formed Hägg carbide was substantially greater for spinel with a smaller specific surface [11].

Depending on the variety of the wood pulp and type of soils, the elemental compositions of charcoals can differ both qualitatively and quantitatively. The composition of charcoals often includes negligible amounts of impurity metals (1–3 wt %) that are used as the promoters for the catalytic hydrogenation reaction of CO. The most common and widely used promoters of iron-containing catalysts for FTS are potassium and copper. It has therefore been shown that in CMs based on the wood pulp of sea buckthorn, the concentration of potassium was initially around 2 wt % [12]. It is known that potassium affects the adsorption of CO and H_2 molecules in iron-containing catalysts, thereby slowing growth of the strength of Fe–C bonds and weakening the Fe–H bonds [13]. Potassium accelerates the formation of iron carbide, increases its concentration, and substantially affects its activity and selectivity in FTS [14, 15].

Khodakov et al. [16] have shown that a high degree of reduction of the catalyst is achieved and carbidizing of iron nanoparticles increases after the activation of iron-containing carbon nanotubes promoted by Bi and Pb. Strong migration of bismuth and lead was observed during the activation of the catalyst, and it was noted that iron carbide nanoparticles are decorated by promoting elements after activation. Close contact between Fe and promoters was ensured during activation of the catalyst due to the low melting points and high mobility of the metallic promoters [16].

In this work, we studied the dynamics of the carbidizing of Fe-containing bismuth-promoted catalysts based on C_{Am} carbon material obtained from plant biomass, shadbush wood pulp, and a C_{Am} + AMS mechanical mixture (where AMS is aluminum magnesium spinel) in the hydrogenation of CO (CO/H_2).

EXPERIMENTAL

Preparing the Catalysts

Carbon material (CM) (C_{Am}) based on plant biomass, (shadbush wood pulp) and a mixture of the CM with aluminum magnesium spinel (AMS) were chosen as our substrates for Fe-containing catalysts. The shadbush wood pulp was ground to a powder with particle sizes of 0.1–0.25 mm, dried to a constant weight at 110°C, and pyrolysized at 400°C in an air flow. The 2 resulting charcoal was chemically activated in a solution of K_2CO_3 to form anisotropic carbon compounds with different physical properties in the longitudal and transverse layers of the structure and multiply rinsed of potassium ions with hot distilled water with subsequent drying for 5 h in air at 90°C. Calcination was performed in a programmed mode for 3 h in a nitrogen atmosphere at 450°C (the flow rate of gaseous nitrogen was 10 mL/s). Prior to use, the substrates were thoroughly ground in an agate mortar, and fractions with $d < 0.08$ mm were collected. Puralox MG 30 Spinel aluminum magnesium stoichiometric spinel with the formula $Al_xMg_yO_z$ (SASOL GmbH, Germany) with $S_{sp} = 23$ m^2/g of the same fraction of <0.08 mm was used. The technical characteristics of spinel $Al_xMg_yO_z$ were described in [17].

A C_{Am} + AMS mixture was prepared by thoroughly mixing the components at a weight ratio of 1 : 1 on a laboratory vibrating mill and grinding them in an agate mortar with subsequent calcination in a programmed mode for 3 h in a nitrogen atmosphere at 450°C. The catalysts were prepared by applying iron ($Fe(NO_3)_3 \cdot 9H_2O$) and bismuth ($Bi(NO_3)_3 \cdot 5H_2O$) nitrates onto preliminarily prepared substrates via impregnation calculated as 15 wt % iron and 0.6 wt % bismuth in each sample. They were then calcinated in a programmed mode for 3 h in a nitrogen atmosphere at 450°C to decompose the metal nitrates. The catalysts were denoted as Fe/C_{Am}, $FeBi/C_{Am}$, $Fe/(C_{Am}$ + AMS), and $FeBi/(C_{Am}$ + AMS).

Data from our physicochemical studies of all samples of the catalysts via scanning electron microscopy (SEM), energy dispersive analysis (EDA), the low-temperature adsorption of nitrogen, infrared (IR) spectroscopy, and differential thermal analysis (DTA/TGA) were presented in detail in [17].

X-Ray Diffraction (XRD) Spectra

Our samples of the catalysts were additionally analyzed on a Shimadzu XRD-7000 S X-ray diffractometer in the form of layers of powder 1 mm thick and around 20 mm in diameter. A nonreflecting holder with the speed of 30 rpm was used. The optical scheme of the goniometer was θ–θ, and the detector was a scintillator equipped with a monochromator. The operating parameters of the X-ray tube were an accelerating potential of 40 kV, a current of 30 mA, and Cu as the target material. The range of scanning according to angle 2θ was 10° to 95°, the speed of scanning was 1 deg/min, and the step was 0.02°. Correspondence of the X-ray diffraction patterns was sought in the PDF-2 database (Powder Diffraction File PDF-2 Release 2010, International Centre for Diffraction Data).

Table 1. Magnetic characteristics of the catalysts

Sample	J_s	J_r	H_c	Fe_3O_4, wt %	J_s	J_r	H_c	χ-Fe_5C_2/ε'-$Fe_{2.2}C$, wt %
	before the activation in CO/H_2				after the activation in CO/H_2			
Fe/C_{Am}	130.0	6.4	48.0	14.0	286.0	56.0	404.0	20.0
$FeBi/C_{Am}$	172.0	12.0	54.0	19.0	260.0	85.0	617.0	18.0
$Fe/(C_{Am}$ + AMS)	92.0	15.0	76.0	20.0	58.0	29.0	626.0	6.6/1.4
$FeBi/(C_{Am}$ + AMS)	134.0	14.0	82.0	27.0	213.0	64.0	423.0	25.4/1.6

J_s and J_r, G cm^2 g^{-1}; H_c, kE. Calculated wt % of the product: m $Fe_3O_4 = J_s/J°$ Fe_3O_4, where $J°$ Fe_3O_4 = 90 G cm^2 g^{-1}; m $Fe_5C_2 = J_s/J°$ Fe_5C_2, where $J°$ Fe_5C_2 = 144 G cm^2 g^{-1} and $J°$ ε'-$Fe_{2.2}C$ = 160 G cm^2 g^{-1}. J_s is the saturation magnetization, J_r is the residual magnetization, and H_c is the value of the magnetic field.

In Situ Magnetometry

Magnetometry includes a number of items: temperature-programmed reduction (TPR) with simultaneous recording of magnetization (in situ), a thermomagnetic curve (TMC), and magnetic granulometry (field dependences).

Temperature-programmed reduction with simultaneous recording of the magnetization of samples was performed on an original vibrating magnetometer (a laboratory unit) in the in situ mode to measure the magnetization of the ferromagnetic components formed during the chemical reaction [18]. Iron, magnetite, and carbides have considerable magnetic moments that determine the magnetization of samples. During a process, magnetization J changes with temperature, allowing us to monitor the dynamics of reduction over time $J(t)$, and it is proportionate to the weight of the magnetic [19]. In situ magnetometric measurements allow us to determine quite accurately the composition of the extremely unstable iron carbides that form during chemical transformations.

Catalysts with weights of 10–15 mg were reduced in a flow of synthesis gas with the composition $CO : H_2$ = 1 : 1 upon heating to 600°C in the measuring cell of a vibrating magnetometer at a rate of 10 K/min. The cell of the vibrating magnetometer was a flow-type quartz microreactor with a volume of 0.3 cm^3 that allowed us to study topochemical transformations under in situ conditions [19]. The gases were preliminarily passed through a column with γ-Al_2O_3 heated to 300°C to purify them of iron carbonyls. Each sample was immobilized between two membranes made of porous quartz. Upon heating, the change in the magnetization was recorded continuously with a frequency of 1 Hz. Upon reaching the predetermined temperature of 600°C, the catalyst was exposed in the isothermal mode to a constant value of magnetization that marked the end of the reduction process.

The thermomagnetic curve was obtained by reducing the samples in the synthesis gas. They were cooled at a rate of 10°/min in a flow of reducing gas CO/H_2 that was later replaced with argon, and the specific magnetization was measured depending on temperature. The resulting thermomagnetic dependences allowed us to determine the Curie point of the phase being formed with quite high accuracy. The Curie point lay at the intersection between a straight line tangent to the point of maximum velocity of the drop in magnetization and the abscissa axis. The kinks in the thermomagnetic curve showed there were several magnetic phases. The type of each magnetic phase could in this case be determined by the position of the kink in the curve according to the Curie point. Analysis of the thermomagnetic curves when there were two magnetic phases allowed us to determine the quantitative composition of the magnetic phases in the sample [19].

Granulometry was used to determine the magnetic characteristics of the systems from the dependence of magnetization J on the value of magnetic field H (dependence J–H, where J is the specific magnetization in relative units normalized to one gram of the sample and H is the value of the magnetic field in kE–field dependences or hysteresis loops). Table 1 presents the magnetic characteristics of the initial samples at T_r before and after activation at 600°C in a synthesis gas atmosphere.

RESULTS AND DISCUSSION

Figure 1 presents the diffraction patterns of the samples of Fe/C_{Am}, $FeBi/C_{Am}$, $Fe/(C_{Am}$ + AMS), and $FeBi/(C_{Am}$ + AMS). The obtained diffraction patterns were compared to one another, and analysis of the spectra showed that the main crystalline components of the samples of Fe/C_{Am} and $FeBi/C_{Am}$ were magnetite Fe_3O_4 and maghemite as the most suitable modification of iron oxide Fe_2O_3. For $Fe/(C_{Am}$ + AMS) and $FeBi/(C_{Am}$ + AMS), the main crystalline components were modifications of magnetite Fe_3O_4, one that was common with crystal lattice parameter a = 8.396 Å and one that existed at high pressure with crystal lattice parameter a = 8.0903 Å. We found it impossible to

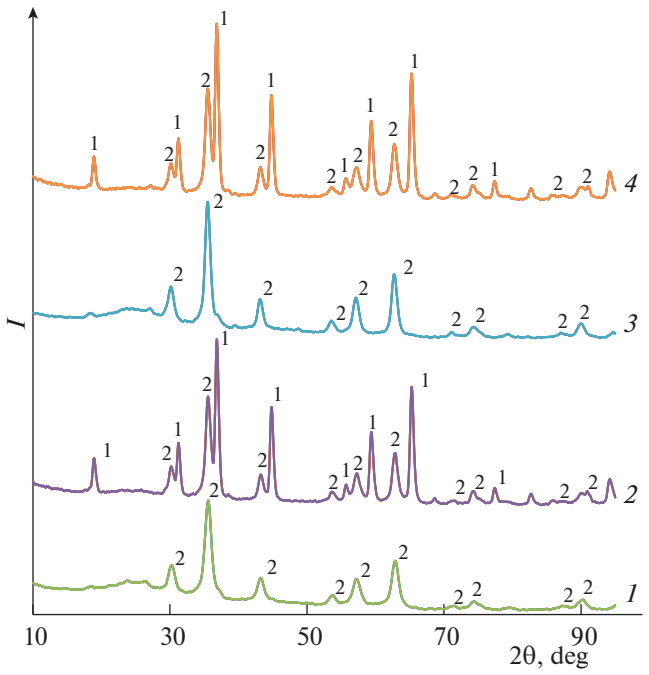

Fig. 1. Results from our X-ray diffraction analysis of samples of (*1*) Fe/C_{Am}, (*2*) FeBi/C_{Am}, (*3*) Fe/(C_{Am} + AMS), and (*4*) FeBi/(C_{Am} + AMS): (*1*) magnetite formed under high pressure (High Pressure Magnetite, 00-026-1136) and (*2*) magnetite (Common Magnetite, 00-019-0629).

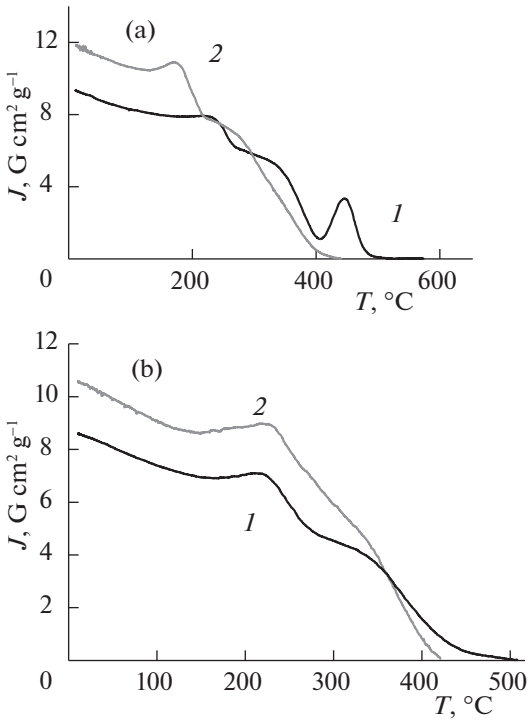

Fig. 2. Dependences of magnetization on temperature during reduction in the medium of synthesis gas CO/H_2 (1 : 1): (a) (*1*) Fe/C_{Am} and (*2*) FeBi/C_{Am} and (b) (*1*) Fe/(C_{Am} + AMS) and (*2*) FeBi/(C_{Am} + AMS).

identify any Bi-containing phases from the database, due apparently to the low concentration of bismuth (0.6 wt %). The presence of magnetite ensured there would be magnetization in the initial samples.

In Situ Magnetometric Measurements

Samples of the catalysts were reduced via in situ magnetometry in a mixture of CO/H_2 at temperatures of up to 600°C. They were heated to a constant value of magnetization, cooled to room *T*, and the thermomagnetic curve was recorded to determine the composition of the resulting products.

Temperature Programmed In Situ Reduction

Figures 2a and 2b show the dependences of the magnetization on temperature during the reduction of Fe/C_{Am}, FeBi/C_{Am}, Fe/(C_{Am} + AMS), and FeBi/(C_{Am} + AMS) in the medium of synthesis gas CO/H_2 (1 : 1). It was noted that dried and calcinated iron-containing catalysts based on activated charcoal already have magnetite in their composition at 350°C [9]. As follows from the XRD data (Fig. 1), the initial catalysts did have nonzero (initial) magnetization at T_r, due to the presence of a magnetic (magnetite). We can see from Figs. 2a,b that the content of magnetite in the bismuth-promoted samples was 25% higher than without bismuth. Upon heating, a drop in magnetization was initially observed that could have been associated with the formation of nonmagnetic thermodynamically unstable wustite with a subsequent rise in magnetization from $T = 130$°C that stopped at $T = 200–230$°C. The magnetization then fell to zero at $T = 430–500$°C. In [19], we showed that the rise in magnetization was due to the formation of magnetite via the reaction $Fe_2O_3 \rightarrow Fe_3O_4$. The subsequent drop in magnetization was induced by the formation of Hägg carbide χ-Fe_5C_2 with Curie point $T_\theta = 257$°C, as is shown below. The additional peak in Fig. 2a in the reduction of Fe/C_{Am} could be associated with postreduction of the fairly small particles of hematite to magnetite.

Two processes can occur simultaneously when $T \geq 257$°C: one is responsible for the growth in magnetization; the other, for its drop. It follows from Fig. 2 that for both Fe/C_{Am} and Fe/(C_{Am} + AMS), promotion with bismuth lowers the temperature of the onset of the reduction of hematite to magnetite, along with that of the formation of carbide. In the latter case, the reduction is more pronounced.

Thermomagnetic Curves

A rise in magnetization was observed after cooling the given samples reduced at 600°C in the synthesis

gas (Figs. 3a,b). The resulting dependences of magnetization on temperature in an inert atmosphere were thermomagnetic curves that are characteristic of the composition of the magnetic phases.

Figures 3a,b show the thermomagnetic curves of Fe/C_{Am}, $FeBi/C_{Am}$, $Fe/(C_{Am}$ + AMS), and $FeBi/(C_{Am}$ + AMS). The samples reduced in the synthesis gas and cooled to room temperature (Fig. 3) had initial magnetization due to the presence of a magnetic phase.

As follows from Fig. 3a, Hägg carbide χ-Fe_5C_2 with Curie point $T_\theta = 257°C$ formed after activation of the Fe/C_{Am} and $FeBi/C_{Am}$ catalysts in the synthesis gas. The Curie point was determined graphically from the intersection of the tangent line to the point of the kink in the thermomagnetic curve with the X axis. Note that a kink is clearly seen in the TMC for the $Fe/(C_{Am}$ + AMS) (Fig. 3b) and $FeBi/(C_{Am}$ + AMS) systems (Fig. 3c), which divides the curve into two unequal parts corresponding to different Curie points. The total value of magnetization is thus $J_{total} = J_{\chi\text{-}Fe_5C_2} + J_{\varepsilon'\text{-}Fe_{2.2}C}$, where the Curie point of Hägg carbide is $T_\theta = 257°C$ and that of ε'-$Fe_{2.2}C$ is $T_\theta = 450°C$ [20]. The amounts of carbides formed after the activation of the catalysts were calculated in light of the values of the specific magnetizations: $J_{0\chi\text{-}Fe_5C_2} = 144$ G cm^2 g^{-1} and $J_{0\varepsilon'\text{-}Fe_{2.2}C} = 160$ G cm^2 g^{-1} [21]. The concentration of magnetite in the initial samples was calculated in a similar manner by allowing for $J_{0\,Fe_3O_4} = 90$ G cm^2 g^{-1} [20].

Table 1 presents the magnetic characteristics of samples of Fe/C_{Am}, $Fe/(C_{Am}$ + AMS), $FeBi/C_{Am}$, and $FeBi/(C_{Am}$ + AMS), where H_c is the coercive force, J_s is the saturation magnetization, and J_r is the residual magnetization.

Magnetic Granulometry

The use of magnetic granulometry allowed us to determine the amounts of the products that formed: $m = I_s/I°$, where $I°$ is the specific value of the magnetization of both magnetite and Hägg carbide.

Figures 4a,b show the field dependences or hysteresis loops for the systems (a) Fe/C_{Am}, $FeBi/C_{Am}$ and (b) $Fe/(C_{Am}$ + AMS) and $FeBi/(C_{Am}$ + AMS), based on which the values of H_c, J_s, and J_r were calculated. It follows from Fig. 4b that the saturation magnetization of the sample of $FeBi/(C_{Am}$ + AMS) was 350% higher than that of the catalyst not promoted by bismuth, which testifies to the high degree of reduction and carbidizing of $FeBi/(C_{Am}$ + AMS) caused by the promoting effect of bismuth (Table 1).

The data presented in Table 1 confirm that prior to activation in the synthesis gas, the promotion of both Fe/C_{Am} and $Fe/(C_{Am}$ + AMS) by bismuth increases the amount of magnetite in the sample.

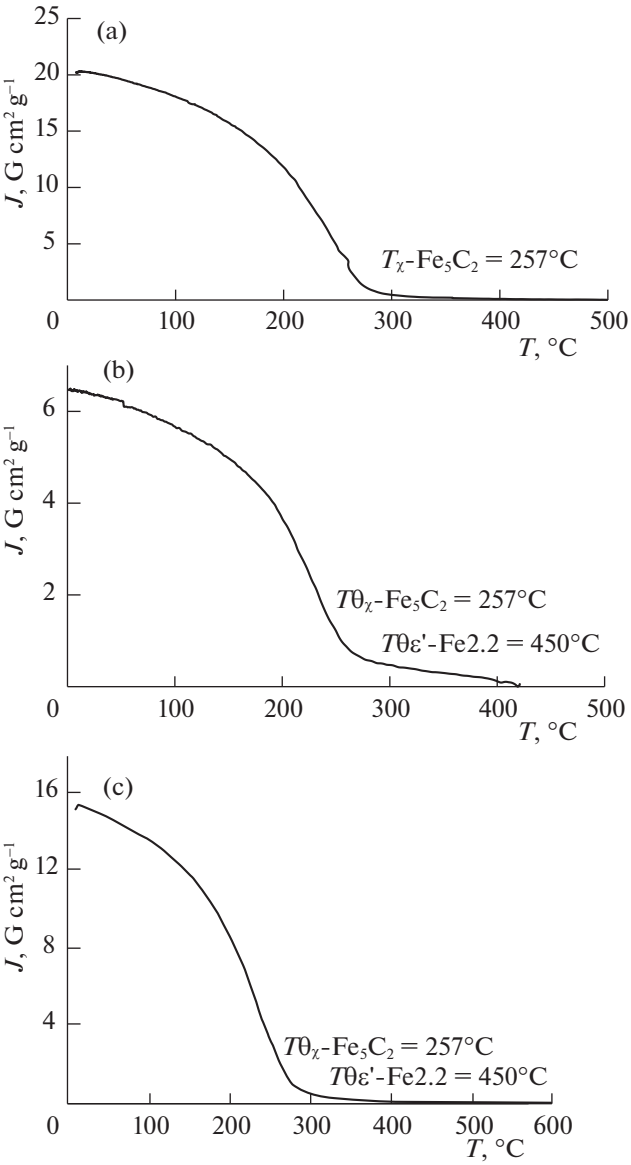

Fig. 3. Thermomagnetic curves: (a) Fe/C_{Am}, (b) $Fe/(C_{Am}$ + AMS), and (c) $FeBi/(C_{Am}$ + AMS).

As follows from Figs. 3a, 3b and data of Table 1, only Hägg carbide forms upon activation of the Fe/C_{Am} catalyst in the synthesis gas, while the promotion of the Fe/C_{Am} catalyst by bismuth had no effect on the amount of formed Hägg carbide. With the activation of the $Fe/(C_{Am}$ + AMS) catalyst in the synthesis gas, ε'-$Fe_{2.2}C$ formed along with χ-Fe_5C_2. However, the promotion of the $Fe/(C_{Am}$ + AMS) catalyst by bismuth increased the amount of Hägg carbide χ-Fe_5C_2 by almost 400% (6.6 and 25.4 wt %) while negligibly affecting the amount of ε'-$Fe_{2.2}C$ (1.4 and 1.6 wt %) in the samples.

To determine how much iron was transformed into magnetite during preparation and to carbides during activation, we used the formula

$$C = cA_{Fe}/M,$$

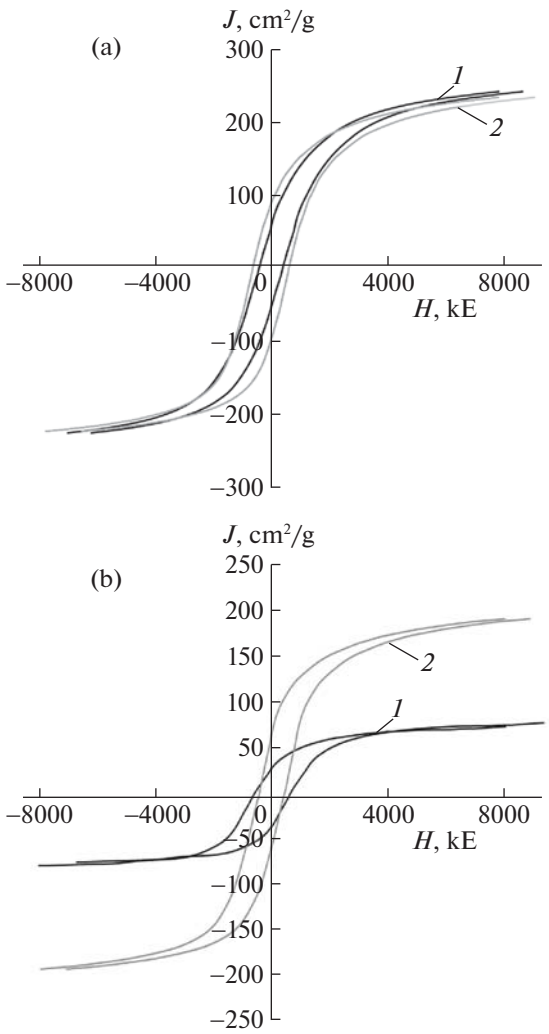

Fig. 4. Field dependences (hysteresis loops): (a) (*1*) Fe/C_{Am} and (*2*) $FeBi/C_{Am}$ and (b) (*1*) $Fe/(C_{Am} + AMS)$ and (*2*) $FeBi/(C_{Am} + AMS)$.

where C is the calculated concentration of Fe in magnetite, χ-Fe_5C_2, or ε'-$Fe_{2.2}C$ according to the data from granulometry, wt %; c is the concentration of magnetite, χ-Fe_5C_2, or ε'-$Fe_{2.2}C$ in the sample, wt %, according to the data of Table 1; A_{Fe} is the concentration of Fe in magnetite, χ-Fe_5C_2, or ε'-$Fe_{2.2}C$ in 1 mol (168, 280, 112, respectively); and M is the molecular weight of magnetite, χ-Fe_5C_2, or ε'-$Fe_{2.2}C$.

The results for the calculated value of Fe in magnetite, χ-Fe_5C_2, and ε'-$Fe_{2.2}C$ in the samples, wt %, are presented in Fig. 5. The analysis in Fig. 5 and comparison of the calculated value of C and concentration of iron in the initial sample at the stage of preparation showed that 60–70% magnetite was present in the Fe/C_{Am} and $FeBi/C_{Am}$ catalysts, and the rest was hematite. It is revealing that the $Fe/(C_{Am} + AMS)$ and

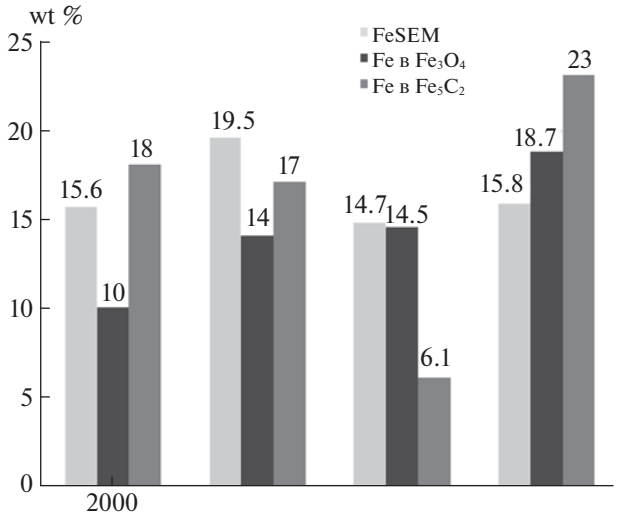

Fig. 5. Concentration of Fe, wt %: (left to right) in the initial sample according to the EDA and SEM data, calculated for Fe_3O_4 using the granulometry data, and for χ-Fe_5C_2 and ε'-$Fe_{2.2}C$ using the granulometry data for samples of (*1*) Fe/C_{Am}, (*2*) $FeBi/C_{Am}$, (*3*) $Fe/(C_{Am} + AMS)$, and (*4*) $FeBi/(C_{Am} + AMS)$.

$FeBi/(C_{Am} + AMS)$ catalysts consisted entirely of magnetite.

$$Fe_3O_4(Fe_2O_3) \begin{array}{l} \rightarrow \chi\text{-}Fe_5C_2 \quad (Fe/C_{Am} \text{ and } FeBi/C_{Am}) \\ \rightarrow \chi\text{-}Fe_5C_2 + \varepsilon'\text{-}Fe_{2.2}C \quad (Fe/(C_{Am} \\ \quad + AMS) \text{ and } FeBi/(C_{Am} + AMS)). \end{array}$$

While the conversion to carbides is 100% for the $FeBi/(C_{Am} + AMS)$ catalyst, however, calculations show it is just 50% for $Fe/(C_{Am} + AMS)$. This is because the concentrations of iron in the initial samples (Fig. 5) can differ from the calculated values, since energy dispersive analysis is a surface-oriented technique. In addition, the structure of the samples of $Fe/(C_{Am} + AMS)$ and $FeBi/(C_{Am} + AMS)$ is spongy, and iron can partially penetrate into the surfaces of the catalysts as we showed in [17]. However, the presence of bismuth stimulates the formation of carbides and apparently promotes their localization on the samples' surfaces, thus making them accessible for quantification. Figure 5 (a histogram) presents the results from calculating the concentrations of Fe in our samples of Fe/C_{Am}, $FeBi/C_{Am}$, $Fe/(C_{Am} + AMS)$ and $FeBi/(C_{Am} + AMS)$.

CONCLUSIONS

In preparing Fe/C_{Am}, promotion by bismuth increases the concentration of magnetite by 32%. The figure for $Fe/(C_{Am} + AMS)$ is 28%, which further facilitates the reduction of the catalysts to carbides. As follows from the data presented in Table 1, only Hägg

carbide χ-Fe_5C_2 (20 wt %) formed after activating the sample of Fe/C_{Am} in the synthesis gas mixture, and promotion by bismuth had almost no effect on the amount of Hägg carbide that formed (18 wt %). With $Fe/(C_{Am}$ + AMS), adding bismuth substantially increased the amount of Hägg carbide that formed (by 400%) and affected the amount of ε'-$Fe_{2.2}C$ carbide negligibly. We can see from Figs. 2a,b that the reduction of $FeBi/C_{Am}$ and $FeBi/(C_{Am}$ + AMS) to carbides stopped at 420–440°C, while it continued up to 500°C and above in the absence of the promoter, bismuth.

It should be noted that it is unlikely bismuth ferrite $BiFeO_3$ would form under the selected conditions of the experiments, since ferrite nanoparticles only start to emerge at 600°C [22]. The presence of bismuth localized on the surface of the substrate probably strengthens the Fe–C bonds. At the same time, the Fe–H bond is weakened, which positively affects the formation of carbides. IR spectroscopy shows that subcarbonyl and bridge forms of adsorption were active on the surface of the sample of $FeBi/C_{Am}$ after activation in a CO atmosphere, which substantially facilitated the reduction of iron oxides [17]. It is also important that a much larger amount of Hägg carbide formed during activation in the synthesis gas when using spinel $Al_xMg_yO_z$, which has a specific surface an order of magnitude smaller (23 m^2/g) than that of aluminum magnesium spinel with a specific surface of 185 m^2/g (Sasol), as a support for the Fe-containing catalyst [11].

REFERENCES

1. F. Marquez-Montesinos, T. Cordero, J. Rodriguez-Mirasol, and J. J. Rodriguez, Sep. Sci. Technol. **36**, 3191 (2001).
2. B. Faug, Microporous Mesoporous Mater. **182**, 1 (2013).
3. C. S. Castro, M. C. Guerreiro, L. C. A. Oliveira, et al., Appl. Catal., **A367**, 53 (2009).
4. P. A. Chernavskii and V. V. Lunin, Zh. Fiz. Khim. **34**, 531 (1994).
5. T. J. Bandosz, *Activated Carbon Surfaces in Environmental Remediation* (Elsevier, New York, 2006).
6. B. H. Davis, Catal. Today **141**, 25 (2009).
7. F. Jiang, M. Zhang, B. Liu, et al., Catal. Sci. Technol. **7**, 1245 (2017).
8. M. E. Dry, in *Studies in Surface Science and Catalysis,* Ed. by A.P. Steynberg and M. E. Dry (Elsevier, Amsterdam, 2004), **Vol. 152**, p. 533.
9. V. V. Ordomsky, B. Legras, K. Cheng, et al., Catal. Sci. Tech. **5**, 1433 (2015).
10. J. M. Gracia, F. F. Prinsloo, and J. W. Niemantsverdri- 1 et, Catt. Lett. **133**, 257 (2009).
11. G. V. Pankina, A. V. Shumyantsev, S. A. Chernyak, and V. V. Lunin, Kinet. Catal. **60**, 672 (2019).
12. G. V. Pankina, P. A. Chernavskii, and V. V. Lunin, Russ. J. Phys. Chem. A **90**, 1743 (2016).
13. V. R. R. Penduala, U. M. Graham, G. Jacobs, et al., Catal. Lett. **144**, 1704 (2014).
14. H. Wan, B. Wu, C. Zhang, H. Xiang, Y. Li, J. Mol. Catal. **283**, 33 (2008).
15. P. A. Chernavskii, V. O. Kazak, G. V. Pankina, N. E. Strokova, and Yu. D. Perfil'ev, Kinet. Catal. **59**, 229 (2018).
16. B. Gua, V. V. Ordomsky, M. Bahri, et al., Appl. Catal. B: Environ. **234**, 153 (2018).
17. G. V. Pankina, P. A. Chernavskii, and V. V. Lunin, Russ. J. Phys. Chem. A (2020, in press).
18. P. A. Chernavskii, B. S. Lunin, R. A. Zakharyan, et al., Instrum. Exp. Tech. **57**, 78 (2014).
19. P. A. Chernavskii, G. V. Pankina, and V. V. Lynin, Russ. Chem. Rev. **80**, 579 (2011).
20. P. W. Selwood, *Magnetochemistry* (Interscience, New York, 1956).
21. G. L. Zhang, Y. C. Lin, X. Chen, and N. Y. Goo, J. Hazard. Mater. **148**, 671 (2007).
22. X. Wang, C. Yang, D. Zhou, et al., Chem. Phys. Lett. **713**, 185 (2018).

Translated by E. Boltukhina

SPELL: 1. Niemantsverdriet, 2. pyrolysized